



Phase equilibria and thermodynamic calculation of the Co–Ta binary system



Kazuya Shinagawa, Hibiki Chinen, Toshihiro Omori, Katsunari Oikawa, Ikuo Ohnuma*, Kiyohito Ishida, Ryosuke Kainuma

Department of Materials Science, Graduate School of Engineering, Tohoku University, Sendai 980-8579, Japan

ARTICLE INFO

Article history:

Received 22 October 2013

Received in revised form

19 January 2014

Accepted 22 January 2014

Available online 15 February 2014

Keywords:

A. Intermetallics, miscellaneous

A. Laves phases

B. Phase diagrams

B. Order/disorder transformations

D. Microstructure

E. Phase diagram, prediction

ABSTRACT

Experimental investigation and thermodynamic evaluation of the Co–Ta binary phase diagram was carried out. Equilibrium compositions obtained in two-phase alloys and diffusion couples were measured by electron probe microanalyzer (EPMA). A very narrow λ_3 (C36) + λ_2 (C15) two-phase region is confirmed to be present around 26.5 at.% Ta at temperatures between 950 °C and 1448 °C. Equilibrium relationships above 1500 °C among the liquid, Laves (λ_1 (C14), λ_2 and λ_3 , whose stoichiometry is described by Co_2Ta), μ (D8_b) and CoTa_2 (C16) phases were investigated by microstructural examination in as-cast Co-(24–60 at.%)Ta alloys. The solvus temperature of the γ' Co_3Ta (L1₂) phase precipitated in the 5.8 at.%Ta γ (Co) and the peritectoid temperature of the Co_7Ta_2 phase in an 8.5 at.%Ta alloy were determined to be 1013 °C and 1033 °C, respectively, by differential scanning calorimeter (DSC). Fine precipitates of the γ' phase precipitated in the γ (A1) matrix were observed by transmission electron microscope (TEM). Analyzing the present experimental results synthetically, the γ' Co_3Ta phase was identified to be a metastable phase, of which the γ/γ' transition temperature of the stoichiometric Co_3Ta alloy was estimated to be 2000 °C. Thermodynamic assessment of the Co–Ta binary system was carried out based on the present results as well as on experimental data in the literature. Calculated results of not only stable but also metastable equilibria were found to be in good agreement with the revised phase diagram. The evaluated stability of the metastable γ' Co_3Ta coincides with the enthalpy of formation ($\Delta H(\gamma'\text{Co}_3\text{Ta}) = -23.44$ kJ/mol) calculated by the *ab initio* method.

© 2014 Elsevier Ltd. All rights reserved.

1. Introduction

Conventional Co-base superalloys, which are widely applied in chemical plants, power generation systems, and so on [1], are basically strengthened by precipitation hardening by carbides and by solid solution hardening with heat-resistant elements, such as Cr, Mo, W, Ta, and others. Compared with these strengthening methods, the coherent precipitation of the geometrically close-packed (GCP) phases, such as the γ' phase with an L1₂ structure, is expected to have superior effects on the mechanical properties because it has been practically applied in Ni-base superalloys. Therefore, if coherent γ' particles can be precipitated in the Co-base matrix, the heat-resistant and mechanical properties of the Co-base alloys are expected to surpass those of the Ni-base superalloys because the melting temperature of Co (1492 °C) is 39 °C higher

than that of Ni (1453 °C). In the Co-base binary systems, the stable γ' phase appears only in the Co–Ti system, which has resulted in extensive investigations of Co–Ti-base alloys. However, the low melting temperature of the γ' Co_3Ti phase below 1200 °C as well as the inadequate lattice constant for coherent precipitation prevents Co–Ti-base alloys from being utilized for practical applications. In other Co-base binary systems, Co–Al [2–4], Co–Ta [5,6] and Co–W [7,8], the existence of the metastable γ' phase was reported. However, the phase stability of the $\gamma'\text{Co}_3\text{X}$ phases in each system is so low that they easily disappear through transformation into stable phases at high temperatures. Therefore, Co-base superalloys strengthened by γ' precipitates have not been successfully applied as practical materials.

Recently, Sato et al. [9] found a microstructure similar to that of Ni-base superalloys, that is, cuboidal $\gamma'\text{Co}_3(\text{Al}, \text{W})$ (L1₂) particles coherently and densely precipitated in Co-rich γ (A1) matrix in the Co–Al–W ternary system. Additionally, the strength of the $\gamma'\text{Co}_3(\text{Al}, \text{W})$ phase shows a positive temperature dependence [10] and its stability is enhanced with increasing Ni content [11]. The

* Corresponding author. Tel.: +81 22 795 7322; fax: +81 22 795 7323.

E-mail address: ohnuma@material.tohoku.ac.jp (I. Ohnuma).

effects of other additional elements, such as Cr, Mo, Nb, Ta and so on, on the stability of the γ' phase have been investigated both experimentally and theoretically [12–15]. Especially, Ta tends to be distributed in the γ' phase, which results in a considerable increase of the γ' solvus temperature compared with other elements [14,15]. Furthermore, both polycrystalline and single-crystal Co–Al–W–Ta alloys with a $\gamma + \gamma'$ two-phase microstructure exhibit considerable strength at elevated temperatures, which indicates that the Co-base alloys have promising potential as next generation superalloys [16]. In order to control the microstructure as well as to optimize heat-treatment conditions, precise information on phase equilibria in the Co base systems and the effect of alloying elements should be understood. However, the phase diagram of the Co–Ta binary system, which was determined by thermal analysis, X-ray diffraction and metallography many years ago, still has room for improvement [17]. Taking into account the above-mentioned situations, the purpose of this study was to determine phase equilibria and to complete thermodynamic assessment of the Co–Ta binary system.

2. Available information

2.1. Phase diagram and crystalline phases

The latest phase diagram of the Co–Ta binary system was assessed by Okamoto [17] as shown in Fig. 1 based on experimental investigations [18–23]. This phase diagram consists of four disordered solution phases, that is, liquid, $\varepsilon(\text{Co})$ (A3), $\gamma(\text{Co})$ (A1) and $\alpha(\text{Ta})$ (A2), three Laves phases, namely, λ_1 (C14), λ_2 (C15) and λ_3 (C36), and other intermetallic compounds, $\chi\text{Co}_7\text{Ta}_2$ (unidentified structure), μ (D8₅) and CoTa_2 (C16). Even though equilibrium relationships among these phases are expected to be complicated, most previous investigations were performed by thermal analysis, X-ray diffraction and metallography [20–22], which might have resulted in insufficient accuracy. For instance, the existence of the λ_1 compound was confirmed in as-cast samples of arc-melted Co–Ta alloys. However, the temperature and composition of the eutectoid reaction $\lambda_1 = \lambda_2 + \mu$ have not been determined experimentally. Therefore, experimental investigations to improve the reliability of phase equilibria in the Co–Ta system are still required.

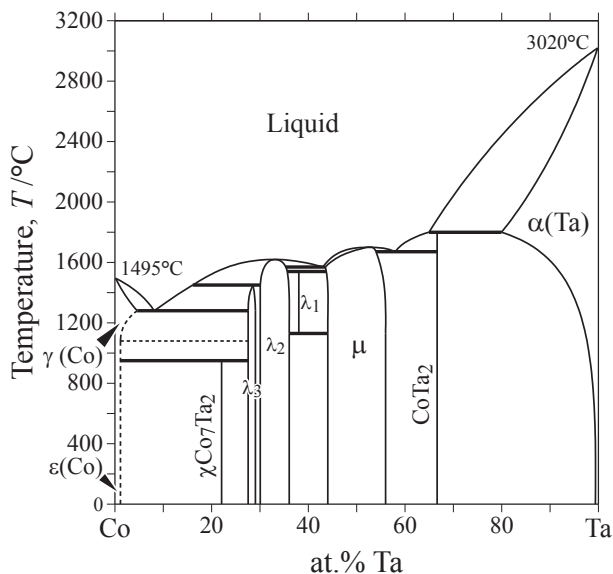


Fig. 1. Phase diagram of the Co–Ta binary system assessed by Okamoto [17].

2.2. Thermodynamic modeling

The first attempt at thermodynamic assessment of the Co–Ta system was carried out by Kaufman [24], in which the enthalpy of formation of intermetallic compound (IMC) phases proposed by Niessen [25] and Colinet [26] was taken into account. In this assessment, all IMC phases were assumed to be stoichiometric line compounds; $\chi\text{Co}_7\text{Ta}_2(\text{Co}_{0.78}\text{Ta}_{0.22})$, $\lambda_3(\text{Co}_{0.75}\text{Ta}_{0.25})$, $\lambda_2(\text{Co}_{0.667}\text{Ta}_{0.333})$, $\lambda_1(\text{Co}_{0.62}\text{Ta}_{0.38})$, $\mu(\text{Co}_{0.5}\text{Ta}_{0.5})$ and $\text{CoTa}_2(-\text{Co}_{0.333}\text{Ta}_{0.667})$. Subsequently, Liu [27] and Hari-Kumar [28] revised the Gibbs energy descriptions of the λ_3 , λ_2 and μ phases to reproduce off-stoichiometric solubility in these compounds. In addition, Hari-Kumar proposed the stoichiometric ratio of the λ_1 and λ_3 Laves phases to be $\text{Co}_{16}\text{Ta}_9$ and Co_3Ta , respectively. However, even though the confirmed composition of these Laves phases deviates from its stoichiometry of Co_2Ta , the thermodynamic description of $(\text{Co,Ta})_2(\text{Co,Ta})$ suggested by Liu is

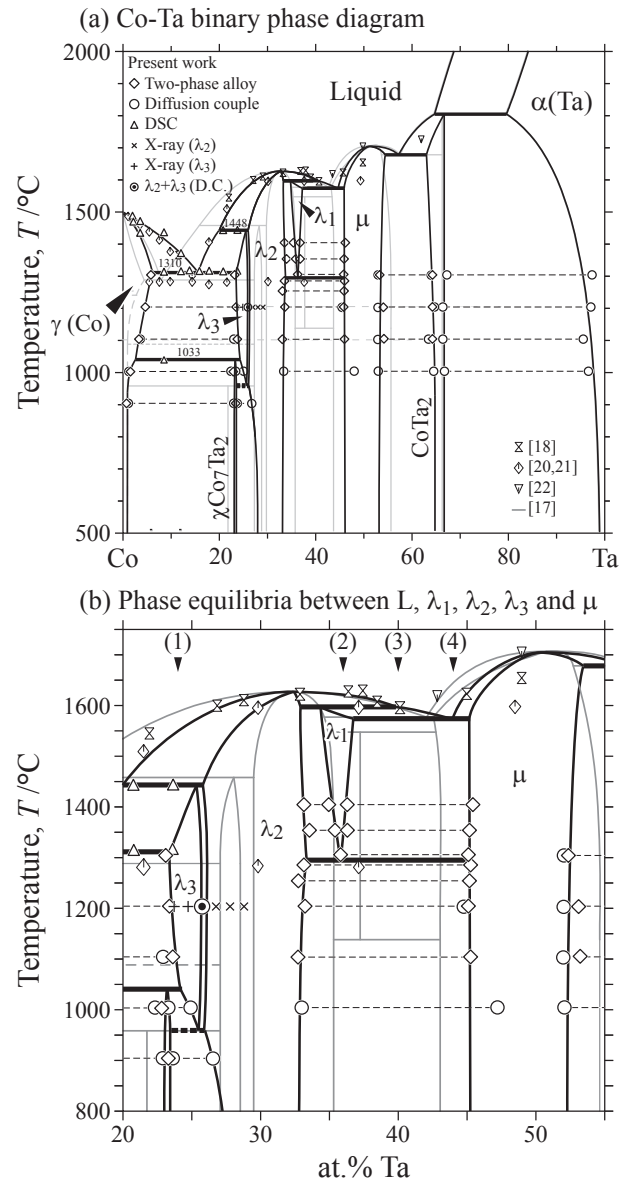


Fig. 2. Phase diagram of the Co–Ta binary system determined by the present work. The previous phase diagram shown in Fig. 1 [17] was superimposed by gray curves.

acceptable. The thermodynamic descriptions of the μ phase were proposed as $(\text{Co})(\text{Ta})$ by Kaufman, $(\text{Co}, \text{Ta})_7(\text{Ta})_2(\text{Co}, \text{Ta})_4$ by Liu and $(\text{Co}, \text{Ta})_1(\text{Co}, \text{Ta})_2(\text{Co})_6(\text{Ta})_4$ by Hari-Kumar. The μ phase also appears in X – Y binary systems ($X = \text{Fe}, \text{Co}, \text{Ni}$ or Zn , $Y = \text{Nb}, \text{Mo}, \text{Ta}$ or W) [29,30]. To extend to multi-component systems involving these elements, a much simpler description with an appropriate solubility range, $(\text{Co})_6(\text{Ta})_4(\text{Co}, \text{Ta})_3$ used in Ni-data database, is preferable rather than pursuing crystallographic exactness.

3. Experimental procedure

Co–Ta alloys with various compositions were prepared from high-purity Co (99.9%) and Ta (99.9%) by arc melting and induction melting under an argon atmosphere. Small pieces of samples were cut from the as-cast ingots. Some of them were sealed in evacuated quartz capsules backfilled with argon gas, homogenized at 1300 °C for 24 h, and equilibrated at temperatures between 900 °C and 1400 °C for durations between 4 and 168 h to obtain multi-phase equilibrium microstructures. Diffusion couples prepared by pressure welding between pure Co and pure Ta were sealed in the same way and heat-treated at temperatures between 900 °C and 1300 °C for 72–840 h. To prevent

sealed samples from reacting with the quartz capsule during heat treatment above 1200 °C, samples were wrapped with tungsten wire. After each heat treatment, samples were quenched in iced water, mounted in epoxy resin, polished mechanically, and etched with a solution of HCl (1N): HNO_3 (1N) = 1:1. Microstructures of as-cast samples, equilibrated samples, and diffusion couples were examined by an optical microscope (OM) and by a field emission scanning electron microscope (FE-SEM, JEOL JSM-6500F). Thin foils of some alloys for transmission electron microstructure (TEM) examination (JEOL JEM-2000EXII) were prepared by a twin-jet method with an electrolyte consisting of one part perchloric acid and four parts ethanol. Equilibrium compositions of equilibrated samples and composition profiles obtained in diffusion couples were measured by an electron probe micro analyzer (EPMA, JEOL JXA-8100). Transition temperatures were determined by a differential scanning calorimeter (DSC, Netzsch DSC-404) with heating and cooling rates of 10 °C/min under high purity argon gas flow. Liquidus and solidus temperatures were determined with the scanning rate of ± 1 °C/min when their difference was small. Flakes of Ti were placed below the sample carrier of the DSC to remove oxygen in the furnace and to prevent samples from being oxidized during measurement.

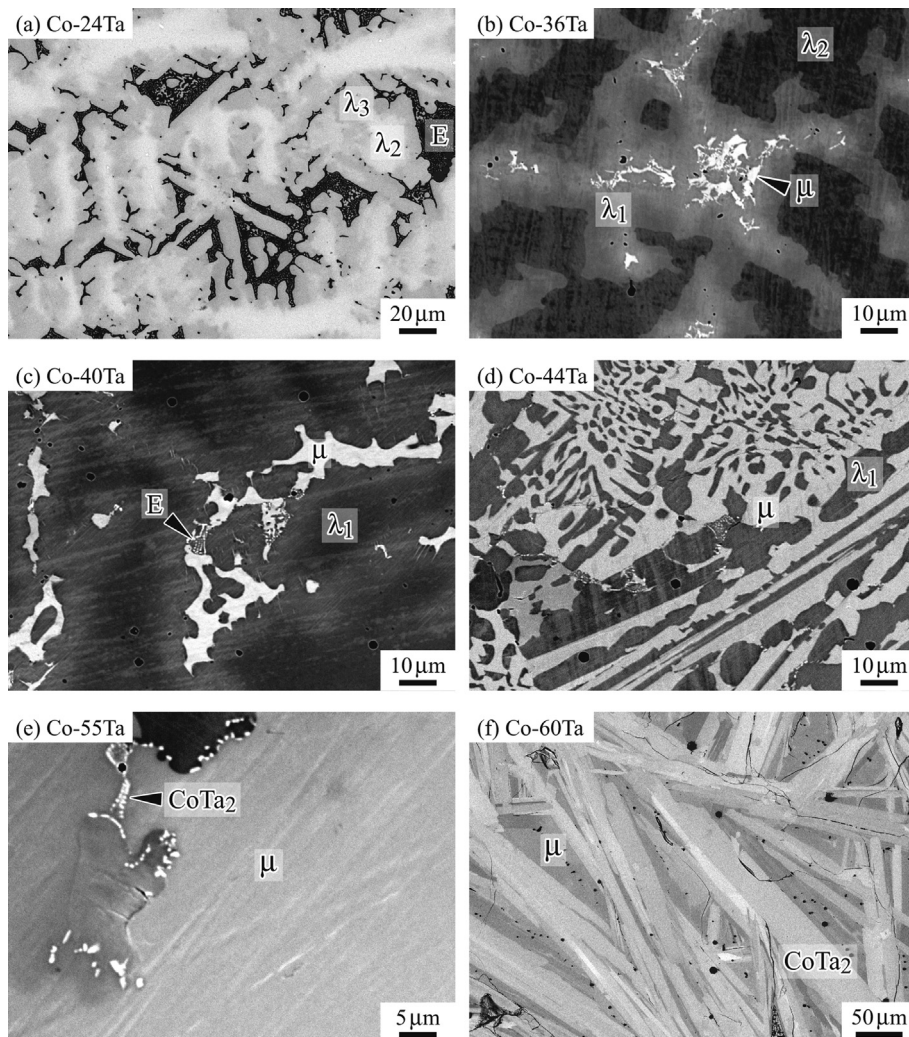


Fig. 3. Back-scattered electron (BSE) images of as-cast microstructure of (a) Co–24Ta, (b) Co–36Ta, (c) Co–40Ta, (d) Co–44Ta (e) Co–55Ta and (f) Co–60Ta (at.%) alloys. “E” represents eutectic microstructure.

4. Thermodynamic modeling

The Gibbs energies of pure elements, so-called lattice stabilities, in stable and metastable structures were taken from the SGTE database compiled by Dinsdale [31]. In the Co–Ta system, four solution phases, that is, liquid, $\varepsilon(\text{Co})$ (A3), $\gamma(\text{Co})$ (A1) and $\alpha(\text{Ta})$ (A2) and seven compound phases, namely, $\gamma'\text{Co}_3\text{Ta}$, $\chi\text{Co}_7\text{Ta}_2$, $\lambda_1(\text{C14})$, $\lambda_2(\text{C15})$, $\lambda_3(\text{C36})$, $\mu(\text{D8}_5)$, CoTa_2 were taken into account for thermodynamic assessment.

4.1. Solution phases

The Gibbs energy of the liquid, $\varepsilon(\text{Co})$ (A3), $\gamma(\text{Co})$ (A1) and $\alpha(\text{Ta})$ (A2) phases was described by sub-regular solution approximation for substitutional solutions using the following equation.

$$G_m^\phi = {}^\circ G_{\text{Co}}^\phi x_{\text{Co}} + {}^\circ G_{\text{Ta}}^\phi x_{\text{Ta}} + RT(x_{\text{Co}} \ln x_{\text{Co}} + x_{\text{Ta}} \ln x_{\text{Ta}}) + x_{\text{Co}} x_{\text{Ta}} L_{\text{Co,Ta}}^\phi + {}^{\text{mag}} G_m^\phi \quad (1)$$

where ${}^\circ G_{\text{Co}}^\phi$ and ${}^\circ G_{\text{Ta}}^\phi$ are the Gibbs energies of pure Co and Ta, respectively, in the corresponding structure of a disordered solution ϕ . x_{Co} and x_{Ta} are the mole fraction of Co and Ta, respectively. $L_{\text{Co,Ta}}^\phi$ represents the interaction parameter which has composition dependence in the form of the Redlich-Kister (RK) polynomial described by the following equation:

$$L_{\text{Co,Ta}}^\phi = \sum_{i=0}^n (x_{\text{Co}} - x_{\text{Ta}})^i \cdot {}^i L_{\text{Co,Ta}}^\phi \quad (2)$$

Coefficients, ${}^i L_{\text{Co,Ta}}^\phi$, were evaluated on the basis of the experimental data on phase boundaries and thermochemical properties. The model of the magnetic contribution to the Gibbs energy formulated by Inden [32,33] – Hillert and Jarl [34] was applied to calculate ${}^{\text{mag}} G_m^\phi$ of the ferro-magnetic ε , γ and α solution phases.

4.2. Intermetallic compounds

4.2.1. γ' Co_3Ta phase

After the Gibbs energy parameters of a disordered fcc phase, $G_m^{\gamma(\text{A1})}(x_s)$, described in the sub-regular solution approximation, were evaluated, the ordering contribution caused by the γ' Co_3Ta (L1₂) structure was implemented by the two-sublattice split compound energy formalism (s-CEF) [35] of the $(\text{Co,Ta})_{0.75}(\text{Co,Ta})_{0.25}$ formula as follows:

$$G_m^{\text{fcc}} = G_m^{\gamma(\text{A1})}(x_s) + G_m^{\gamma(\text{L1}_2)}(y_s^{\text{I}}, y_s^{\text{II}}) - G_m^{\gamma(\text{L1}_2)}(y_s^{\text{I}} = x_s, y_s^{\text{II}} = x_s), \quad (3)$$

where $G_m^{\gamma(\text{L1}_2)}(y_s^{\text{I}}, y_s^{\text{II}})$ is the Gibbs energy described in the two-sublattice compound energy model and $G_m^{\gamma(\text{L1}_2)}(y_s^{\text{I}} = x_s, y_s^{\text{II}} = x_s)$ is a disordered component of $G_m^{\gamma(\text{L1}_2)}(y_s^{\text{I}}, y_s^{\text{II}})$. x_s is the mole fraction of an element s and $y_s^{(n)}$ is the site fraction of the element s on the n -th sublattice. In this formula, only the ordering contribution is extracted from the Gibbs energy of the two-sublattice description of $G_m^{\gamma(\text{L1}_2)}(y_s^{\text{I}}, y_s^{\text{II}})$ by subtracting that of the disordered state of $G_m^{\gamma(\text{L1}_2)}(y_s^{\text{I}} = x_s, y_s^{\text{II}} = x_s)$. In this paper, the ordering contribution of the γ' Co_3Ta (L1₂) structure $\Delta G_{\text{Co}_3\text{Ta}}^{\gamma(\text{L1}_2)}$ is supplemented so as not to have the disordered component, that is, under the condition of $G_m^{\gamma(\text{L1}_2)}(y_s^{\text{I}} = x_s, y_s^{\text{II}} = x_s) = 0$, as follows:

Table 1
Solidification path predicted from as-cast microstructures of Co–Ta alloys.

Sample/at.%	Path 1	Path 2	Path 3
Co–20Ta	$L \Rightarrow L + \lambda_3(\text{C36})$	$L \Rightarrow \gamma(\text{Co}) + \lambda_3$	
Co–21, 22, 24, 26Ta	$L \Rightarrow L + \lambda_2(\text{C15})$	$L + \lambda_2 \Rightarrow \lambda_3$	$L \Rightarrow \gamma + \lambda_3$
Co–36Ta	$L \Rightarrow L + \lambda_2$	$L + \lambda_2 \Rightarrow \lambda_1$	$L \Rightarrow \lambda_1 + \mu$
Co–40, 44Ta	$L \Rightarrow L + \lambda_1(\text{C14})$	$L \Rightarrow \lambda_1 + \mu$	
Co–55Ta	$L \Rightarrow L + \mu$	$L \Rightarrow \mu + \text{CoTa}_2$	
Co–60Ta	$L \Rightarrow L + \text{CoTa}_2$	$L \Rightarrow \mu + \text{CoTa}_2$	

$$G_{\text{Co:Co}}^{\gamma(\text{L1}_2)} = G_{\text{Ta:Ta}}^{\gamma(\text{L1}_2)} = 0 \quad (4.1)$$

$$G_{\text{Co:Ta}}^{\gamma(\text{L1}_2)} = \Delta G_{\text{Co}_3\text{Ta}}^{\gamma(\text{L1}_2)}, \quad G_{\text{Ta:Co}}^{\gamma(\text{L1}_2)} = 0 \quad (4.2)$$

$${}^0 L_{\text{Co:Co,Ta}}^{\gamma(\text{L1}_2)} = -\Delta G_{\text{Co}_3\text{Ta}}^{\gamma(\text{L1}_2)} \quad (4.3)$$

$${}^0 L_{\text{Co,Ta:Co}}^{\gamma(\text{L1}_2)} = 0.25 \Delta G_{\text{Co}_3\text{Ta}}^{\gamma(\text{L1}_2)}, \quad {}^1 L_{\text{Co,Ta:Co}}^{\gamma(\text{L1}_2)} = 0, \\ {}^2 L_{\text{Co,Ta:Co}}^{\gamma(\text{L1}_2)} = -0.25 \Delta G_{\text{Co}_3\text{Ta}}^{\gamma(\text{L1}_2)} \quad (4.4)$$

$${}^0 L_{\text{Co,Ta:Ta}}^{\gamma(\text{L1}_2)} = -1.75 \Delta G_{\text{Co}_3\text{Ta}}^{\gamma(\text{L1}_2)}, \quad {}^1 L_{\text{Co,Ta:Ta}}^{\gamma(\text{L1}_2)} = -\Delta G_{\text{Co}_3\text{Ta}}^{\gamma(\text{L1}_2)}, \\ {}^2 L_{\text{Co,Ta:Ta}}^{\gamma(\text{L1}_2)} = -0.25 \Delta G_{\text{Co}_3\text{Ta}}^{\gamma(\text{L1}_2)} \quad (4.5)$$

$${}^0 L_{\text{Co,Ta:Co,Ta}}^{\gamma(\text{L1}_2)} = \Delta G_{\text{Co}_3\text{Ta}}^{\gamma(\text{L1}_2)} \quad (4.6)$$

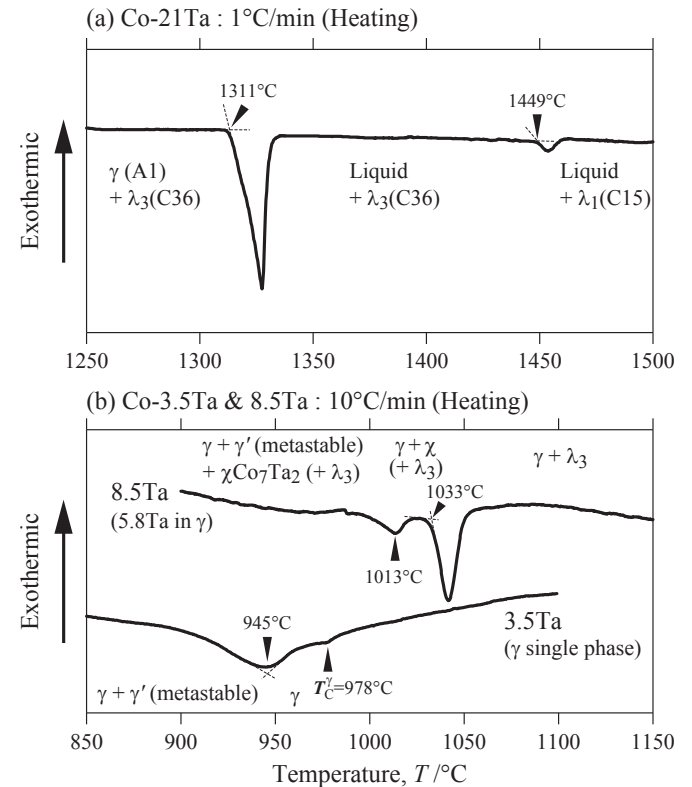


Fig. 4. DSC heating curves measured in (a) Co–21Ta and (b) Co–3.5 and 8.5Ta (at.%) alloys. In the 8.5Ta alloy, phase transformations occurred in the $\gamma(\text{Co})$ matrix phase (5.8at.%Ta) were detected.

Table 2
Phase transformation temperatures ($T_i/^\circ\text{C}$) of Co–Ta alloys.

Sample/at.%	Liquidus	Solidus	$L \Rightarrow \gamma(\text{Co}) + \lambda_3$	$L + \lambda_2(\text{C15}) \Rightarrow \lambda_3(\text{C36})$	$\gamma + \lambda_3 \Rightarrow \chi \text{Co}_7\text{Ta}_2$	$\gamma + \gamma' \text{Co}_3\text{Ta} \Rightarrow \gamma$	T_i^γ
Co–2Ta	1481.1	1462.5					1037.7
Co–3.5Ta	1463.7	1428.5				944.7	977.8
Co–8.5Ta	1429.3		1305.6		1033.0	1013.0 (5.8Ta in γ)	
Co–12Ta	1364.6		1305.0				
Co–14Ta			1311.8				
Co–16Ta			1314.0				
Co–18Ta			1314.0				
Co–21Ta			1310.9	1448.9			
Co–24Ta			1309.0	1447.2			

A unified formula can then be applied to describe the Gibbs energies of both γ (A1) and γ' (L1₂) in the s-CEF as follows:

in which ΔG_f^χ is the Gibbs energy of the formation per mole of atoms of the compound $\chi\text{Co}_7\text{Ta}_2$ expressed by the following equation:

$$G_m^{\text{fcc}} = {}^\circ G_{\text{Co}}^{\gamma(\text{A1})} x_{\text{Co}} + {}^\circ G_{\text{Ta}}^{\gamma(\text{A1})} x_{\text{Ta}} + x_{\text{Co}} x_{\text{Ta}} \left\{ {}^0 L_{\text{Co,Ta}}^{\gamma(\text{A1})} + {}^1 L_{\text{Co,Ta}}^{\gamma(\text{A1})} (x_{\text{Co}} - x_{\text{Ta}}) \right\} + \frac{1}{2} RT \sum_{(n)=1}^{\text{II}} \left(y_{\text{Co}}^{(n)} \ln y_{\text{Co}}^{(n)} + y_{\text{Ta}}^{(n)} \ln y_{\text{Ta}}^{(n)} \right) + y_{\text{Co}}^{\text{I}} y_{\text{Ta}}^{\text{II}} G_{\text{Co:Ta}}^{\gamma(\text{L1}_2)} + y_{\text{Co}}^{\text{I}} y_{\text{Ta}}^{\text{I}} y_{\text{Co}}^{\text{II}} \left\{ {}^0 L_{\text{Co,Ta:Co}}^{\gamma(\text{L1}_2)} + {}^2 I_{\text{Co,Ta:Co}}^{\gamma(\text{L1}_2)} (y_{\text{Co}}^{\text{I}} - y_{\text{Ta}}^{\text{I}})^2 \right\} + y_{\text{Co}}^{\text{I}} y_{\text{Ta}}^{\text{I}} y_{\text{Ta}}^{\text{II}} \left\{ {}^0 L_{\text{Co,Ta:Ta}}^{\gamma(\text{L1}_2)} + {}^1 L_{\text{Co,Ta:Ta}}^{\gamma(\text{L1}_2)} (y_{\text{Co}}^{\text{I}} - y_{\text{Ta}}^{\text{I}}) + {}^2 I_{\text{Co,Ta:Ta}}^{\gamma(\text{L1}_2)} (y_{\text{Co}}^{\text{I}} - y_{\text{Ta}}^{\text{I}})^2 \right\} + y_{\text{Co}}^{\text{I}} y_{\text{Ta}}^{\text{I}} y_{\text{Co}}^{\text{II}} y_{\text{Ta}}^{\text{II}} \cdot {}^0 I_{\text{Co,Ta:Co,Ta}}^{\gamma(\text{L1}_2)} + \text{mag} G_m^{\text{fcc}} \quad (5)$$

The evaluated value of the only one independent thermodynamic parameter to describe the ordering contribution of the γ' Co₃Ta (L1₂) structure, $\Delta G_{\text{Co}_3\text{Ta}}^{\gamma(\text{L1}_2)}$, is listed in Table 4.

$$\Delta G_f^\chi = -33091.5 + 5.16 T \quad (7)$$

4.2.2. Co₇Ta₂

The Gibbs energy of a stoichiometric compound, $\chi\text{Co}_7\text{Ta}_2$, is described as

4.2.3. Laves phase

Three kinds of Laves phases, λ_1 (C14), λ_2 (C15) and λ_3 (C36), appear in the Co–Ta system. The thermodynamic model of all these Laves phases with a considerable solubility range was described by a two-sublattice model of (Co,Ta)₂(Co,Ta). Thus, the Gibbs energy of the Laves phases can be expressed as follows:

$$G_m^{\chi\text{Co}_7\text{Ta}_2} = 0.7778 {}^\circ G_{\text{Co}}^e + 0.2222 {}^\circ G_{\text{Ta}}^e + \Delta G_f^\chi \quad (6)$$

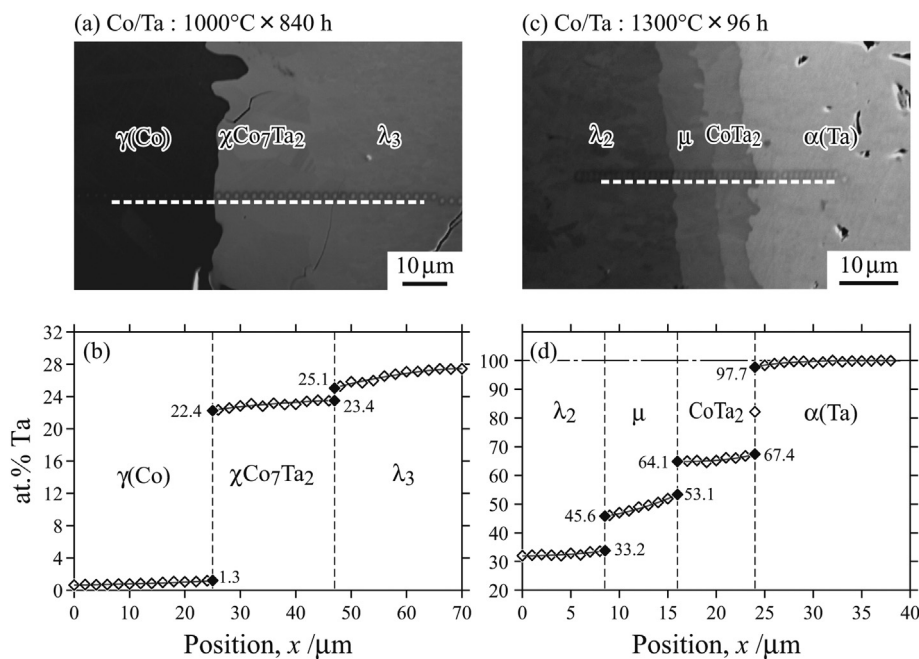


Fig. 5. BSE images and composition profiles measured across inter-phase boundaries of Co/Ta diffusion couples heat-treated at (a), (b) 1000 °C for 840 h and (c), (d) 1300 °C for 96 h.

Table 3
Equilibrium compositions of Co–Ta alloys determined by EPMA.

Sample (at.% Ta) ^a	H.T. temp. ^b (°C)	H.T. period (hours)	Equilibrated phases		Equilibrium composition (at.% Ta)		
			Phase 1	Phase 2	Phase 1	Phase 2	
8.5	900	672	γ (Co)	χ (Co ₇ Ta ₂)	0.7	23.4	
	1000	624	γ	χ	1.5	22.9	
	1100	336	γ	λ_3 (C36)	3.3	23.8	
	1200	278	γ	λ_3	4.6	23.5	
	1300	265	γ	λ_3	5.8	23.2	
36	1350	168	λ_2 (C15)	λ_1 (C14)	34.0	35.9	
	1400	168	λ_2	λ_1	33.6	35.6	
42	1200	168	λ_2	μ	33.6	46.0	
	1250	168	λ_2	μ	33.2	46.0	
	1280	168	λ_2	μ	33.6	46.1	
	1290	168	λ_2	μ	33.6	46.2	
	1300	240	λ_1	μ	36.3	45.9	
	1350	168	λ_1	μ	36.7	42.0	
	1400	168	λ_1	μ	36.8	46.2	
	55	1300	168	μ	CoTa ₂	53.4	64.4
	D.C. ^c	900	672	γ	χ	1.1	23.0
		900	672	χ	λ_3	23.8	26.8
1000		840	γ	χ	1.3	22.4	
1000		840	χ	λ_3	23.4	25.1	
1000		336	λ_2	μ	33.4	48.3	
1000		336	μ	CoTa ₂	52.9	64.7	
1000		336	CoTa ₂	α (Ta)	66.9	96.9	
1100		168	λ_2	μ	33.5	46.1	
1100		168	μ	CoTa ₂	53.0	63.6	
1100		168	CoTa ₂	α	66.6	97.4	
1200		168	λ_2	μ	33.7	47.2	
1200		168	μ	CoTa ₂	53.0	64.8	
1200		168	CoTa ₂	α	66.6	97.4	
1300		96	λ_2	μ	33.2	45.6	
1300		96	μ	CoTa ₂	53.1	64.1	
1300		96	CoTa ₂	α	67.4	97.7	

^a Nominal composition.

^b H.T. represents “heat treatment”.

^c D.C. represents “diffusion couple”.

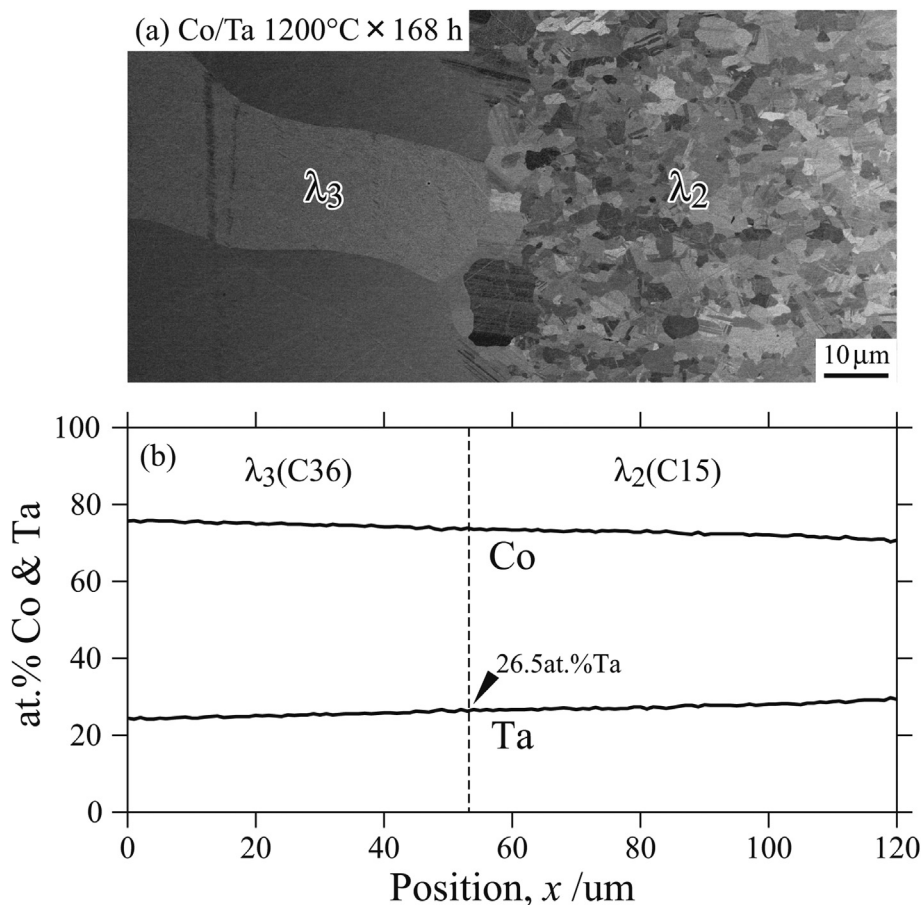


Fig. 6. (a) BSE image of a Co/Ta diffusion couple heat-treated at 1200 °C for 168 h and (b) composition profiles measured across inter-phase boundaries.

$$G_m^{\text{Laves}} = y_{\text{Co}}^{\text{I}} y_{\text{Co}}^{\text{II}} G_{\text{Co:Co}}^{\text{Laves}} + y_{\text{Co}}^{\text{I}} y_{\text{Ta}}^{\text{II}} G_{\text{Co:Ta}}^{\text{Laves}} + y_{\text{Ta}}^{\text{I}} y_{\text{Co}}^{\text{II}} G_{\text{Ta:Co}}^{\text{Laves}} + y_{\text{Ta}}^{\text{I}} y_{\text{Ta}}^{\text{II}} G_{\text{Ta:Ta}}^{\text{Laves}} + 0.6667RT \left(y_{\text{Co}}^{\text{I}} \ln y_{\text{Co}}^{\text{I}} + y_{\text{Ta}}^{\text{I}} \ln y_{\text{Ta}}^{\text{I}} \right) \\ + 0.3333RT \left(y_{\text{Co}}^{\text{II}} \ln y_{\text{Co}}^{\text{II}} + y_{\text{Ta}}^{\text{II}} \ln y_{\text{Ta}}^{\text{II}} \right) + y_{\text{Co}}^{\text{I}} y_{\text{Ta}}^{\text{II}} y_{\text{Co}}^{\text{II}} L_{\text{Co:Co:Ta:Co}}^{\text{Laves}} + y_{\text{Co}}^{\text{I}} y_{\text{Ta}}^{\text{II}} y_{\text{Ta}}^{\text{II}} L_{\text{Co:Ta:Ta}}^{\text{Laves}} + y_{\text{Co}}^{\text{I}} y_{\text{Co}}^{\text{II}} y_{\text{Ta}}^{\text{II}} L_{\text{Co:Co:Ta}}^{\text{Laves}} + y_{\text{Ta}}^{\text{I}} y_{\text{Co}}^{\text{II}} y_{\text{Ta}}^{\text{II}} L_{\text{Ta:Co:Ta}}^{\text{Laves}} \quad (8)$$

4.2.4. μ phase

Several thermodynamic models of the μ phase have been reported [29] because the μ phase has a wide solubility range in various binary systems [30]. A three-sublattice model of $(\text{Co})_6(\text{Ta})_4(\text{Co,Ta})_3$ used in the Ni-data database was adopted in this evaluation because of its simplicity as well as extensibility to the multi-component systems.

$$G_m^{\mu} = y_{\text{Co}}^{\text{III}} G_{\text{Co:Ta:Co}}^{\mu} + y_{\text{Ta}}^{\text{III}} G_{\text{Co:Ta:Ta}}^{\mu} + y_{\text{Co}}^{\text{III}} y_{\text{Ta}}^{\text{III}} L_{\text{Co:Ta:Co:Ta}}^{\mu} \\ + 0.2308RT \left(y_{\text{Co}}^{\text{III}} \ln y_{\text{Co}}^{\text{III}} + y_{\text{Ta}}^{\text{III}} \ln y_{\text{Ta}}^{\text{III}} \right) \quad (9)$$

4.2.5. CoTa_2 phase

The CoTa_2 (C16) phase was described as a line compound with a two-sublattice formula, $(\text{Co})(\text{Ta})_2$, in previous studies [24,27,28]. However, it is apparent that the CoTa_2 phase has a solubility range according to present experimental results. Therefore, the revised two-sublattice model $(\text{Co,Ta})(\text{Co,Ta})_2$ is proposed in this study. The Gibbs energy of the CoTa_2 phase is described by the following equation:

$$G_m^{\text{CoTa}_2} = y_{\text{Co}}^{\text{I}} y_{\text{Co}}^{\text{II}} G_{\text{Co:Co}}^{\text{CoTa}_2} + y_{\text{Co}}^{\text{I}} y_{\text{Ta}}^{\text{II}} G_{\text{Co:Ta}}^{\text{CoTa}_2} + y_{\text{Ta}}^{\text{I}} y_{\text{Co}}^{\text{II}} G_{\text{Ta:Co}}^{\text{CoTa}_2} \\ + y_{\text{Ta}}^{\text{I}} y_{\text{Ta}}^{\text{II}} G_{\text{Ta:Ta}}^{\text{CoTa}_2} + 0.3333RT \left(y_{\text{Co}}^{\text{I}} \ln y_{\text{Co}}^{\text{I}} + y_{\text{Ta}}^{\text{I}} \ln y_{\text{Ta}}^{\text{I}} \right) \\ + 0.6667RT \left(y_{\text{Co}}^{\text{II}} \ln y_{\text{Co}}^{\text{II}} + y_{\text{Ta}}^{\text{II}} \ln y_{\text{Ta}}^{\text{II}} \right) \\ + y_{\text{Co}}^{\text{I}} y_{\text{Ta}}^{\text{I}} y_{\text{Co}}^{\text{II}} L_{\text{Co:Ta:Co}}^{\text{CoTa}_2} + y_{\text{Co}}^{\text{I}} y_{\text{Ta}}^{\text{I}} y_{\text{Ta}}^{\text{II}} L_{\text{Co:Ta:Ta}}^{\text{CoTa}_2} \\ + y_{\text{Co}}^{\text{I}} y_{\text{Co}}^{\text{II}} y_{\text{Ta}}^{\text{I}} L_{\text{Co:Co:Ta}}^{\text{CoTa}_2} + y_{\text{Ta}}^{\text{I}} y_{\text{Co}}^{\text{II}} y_{\text{Ta}}^{\text{II}} L_{\text{Ta:Co:Ta}}^{\text{CoTa}_2} \quad (10)$$

5. Results and discussions

All the results in this work are summarized in Fig. 2. Details of experiments are described below.

5.1. As-cast microstructures

Fig. 3 shows as-cast microstructures of Co–Ta alloys. In the Co–24 at.%Ta alloy shown in Fig. 3(a), the λ_2 phase solidified as a primary crystal, the λ_3 phase formed due to the peritectic reaction ($\text{liquid} + \lambda_2 = \lambda_3$) and then the solidification terminated with the eutectic reaction ($\text{liquid} = \gamma(\text{Co}) + \lambda_3$), which is consistent with the phase diagram shown in Fig. 1 as well as in Fig. 2 (24 at.%Ta is represented by a downward arrow (1) in Fig. 2(b)). As-cast microstructures of 55 at.% Ta (Fig. 3(e)) and 60 at.%Ta (Fig. 3(f)) alloys are also consistent with both of Figs. 1 and 2. On the other hand, in the case of 36, 40 and 44 at.% Ta alloys, shown in Fig. 3(b–d), respectively, results inconsistent with the phase diagram (Fig. 1) were obtained. In the 36 at.%Ta alloy, the solidification started with λ_2 and the peritectic reaction ($\text{liquid} + \lambda_2 = \lambda_1$) followed instead of the eutectic reaction ($\text{liquid} = \lambda_2 + \mu$) predicted from Fig. 1. Finally, a divorced μ -rich eutectic reaction ($\text{liquid} = \lambda_1 + \mu$) occurred. This solidification sequence was confirmed by as-cast microstructures of 40 and 44 at.% Ta alloys, in which the primary crystal was λ_1 .

Solidification paths observed in as-cast 36, 40 and 44 at.% Ta alloys are consistent with the revised phase diagram shown in Fig. 2(b) in which their chemical compositions are superimposed by downward arrows (2), (3) and (4), respectively. Obtained results are summarized in Table 1.

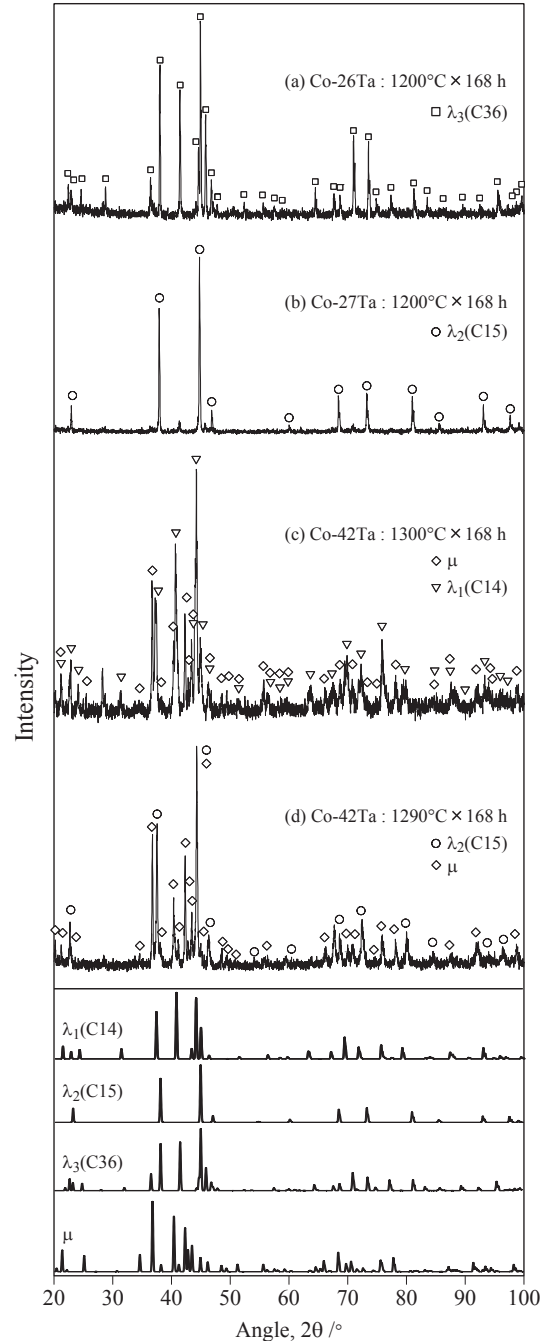


Fig. 7. X-ray diffraction profiles taken from (a) Co–26Ta, (b) Co–27Ta, (c) Co–42Ta and (d) Co–42Ta alloys heat-treated at 1200 °C, 1200 °C, 1300 °C and 1290 °C for 168 h, respectively.

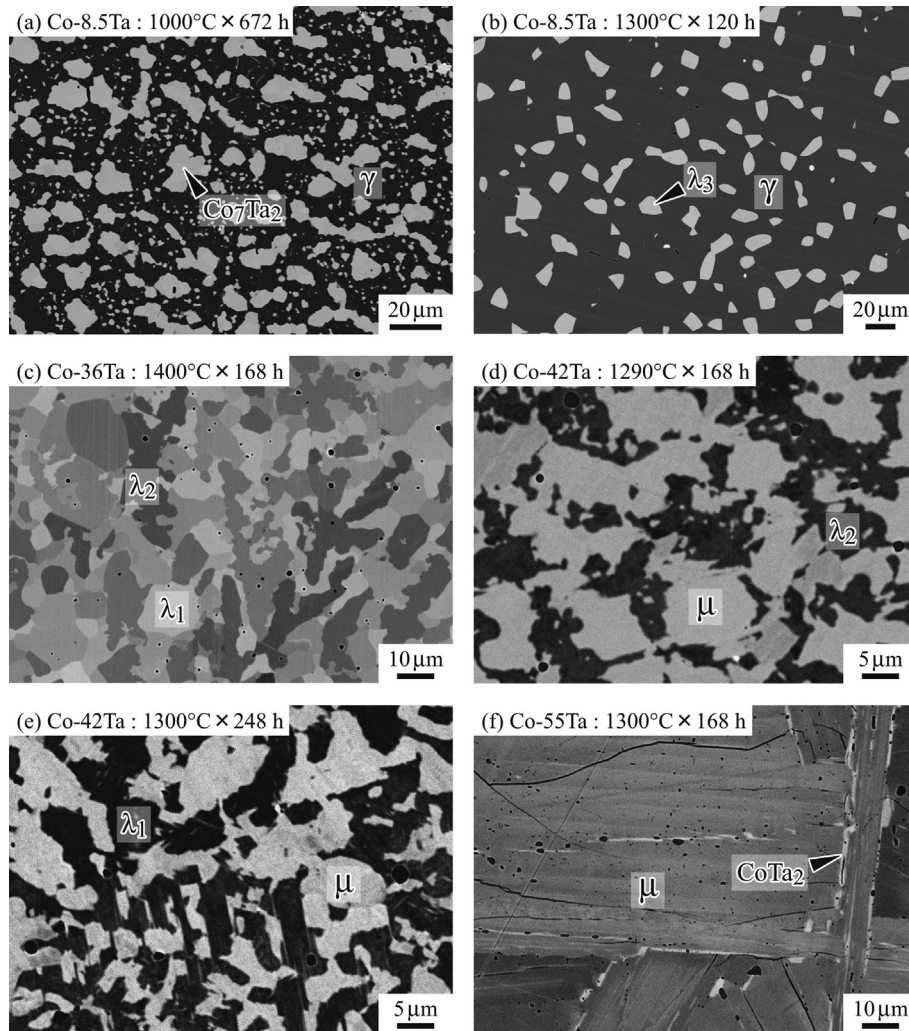


Fig. 8. BSE images of (a) Co-8.5Ta, solution-treated at 1300 °C for 120 h/cold rolled by 50%/equilibrated at 1000 °C for 672 h, (b) Co-8.5Ta equilibrated at 1300 °C for 120 h, (c) Co-36Ta equilibrated at 1400 °C for 168 h, (d) Co-42Ta equilibrated at 1290 °C for 168 h, (e) Co-42Ta equilibrated at 1300 °C for 248 h, and (f) Co-55Ta equilibrated at 1300 °C for 168 h.

5.2. DSC measurement

Fig. 4 shows typical examples of DSC measurement performed on (a) 21 at.%Ta and (b) 3.5 and 8.5 at.%Ta alloys. Two endothermic signals obtained in the 21 at.% Ta shown in Fig. 4(a) are caused by the eutectic reaction, liquid = $\gamma(\text{Co}) + \lambda_3$ at 1311 °C, and the peritectic reaction, liquid + $\lambda_2 = \lambda_3$ at 1448 °C. The revised eutectic temperature (1310 °C) is 30 °C higher than the previous value (1280 °C) shown in Fig. 1. Before the DSC measurement, 3.5 at.%Ta and 8.5 at.%Ta alloys were heat-treated at 1200 °C for 1 h to obtain $\gamma(\text{Co})$ single phase and at 1300 °C for 1 h to obtain $\gamma(\text{Co})$ matrix phase (5.8 at.%Ta) with λ_3 precipitates, respectively. Then, phase transformations occurred in the $\gamma(\text{Co})$ matrix (5.8 at.%Ta) were detected in the 8.5 at.%Ta alloy. In the DSC heating curve of 3.5 at.% Ta alloy shown in Fig. 4(b), a tail of an endothermic reaction was detected at 945 °C. An analogous DSC signal was detected at 1013 °C in 8.5 at.%Ta alloy. These signals seem to have been caused by the dissolution of the metastable $\gamma' \text{Co}_3\text{Ta}$ (L1₂) phase, which will be described in the Section 5.6. In addition, a small endothermic knick-point appeared at 978 °C in 3.5 at.%Ta alloy, which caused by the magnetic transition (Curie temperature, T_C^γ). A sharp endothermic reaction was detected at 1033 °C in 8.5 at.%Ta alloy, which

corresponds to the peritectoid reaction, $\gamma(\text{Co}) + \lambda_3 = \chi\text{Co}_7\text{Ta}_2$. Other DSC results are summarized in Table 2 and plotted in Fig. 2.

5.3. Diffusion couples

Fig. 5 shows microstructures and composition profiles obtained from Co/Ta diffusion couples heat-treated at 1000 °C for 840 h (a), (b) and at 1300 °C for 96 h (c), (d). Composition steps in the profiles corresponding to inter-phase boundaries of $\gamma(\text{Co})/\chi\text{Co}_7\text{Ta}_2$ and $\chi\text{Co}_7\text{Ta}_2/\lambda_3$ in Fig. 5(a), and of λ_2/μ , μ/CoTa_2 and $\text{CoTa}_2/\alpha(\text{Ta})$ in Fig. 5(c) were obtained. Equilibrium compositions were determined by extrapolating the composition profiles from the single-phase region to the inter-phase boundaries, as illustrated by open and solid diamonds in Fig. 5(b and d). The existence of the λ_1 (C14) phase could not be recognized in any diffusion couples. All the data obtained from diffusion couple examinations are summarized in Table 3 and plotted with open circles in Fig. 2.

According to the phase diagram of the Co-Ta system shown in Fig. 1, a narrow equilibrium between λ_3 (29 at.% Ta) and λ_2 (30 at.% Ta) is proposed. However, this equilibrium could not be recognized in any diffusion couples. Instead, an apparent change of polycrystalline microstructure across the composition of 26.5 at.% Ta

was recognized, as shown in Fig. 6(a), in which coarse grains and fine grains were observed at lower and higher Ta contents, respectively. No composition steps could be recognized at the microstructural boundary, as shown in Fig. 6(b). Thus, the crystal structures of Co–Ta alloys below and beyond this composition (26.5 at.%Ta) heat treated at 1200 °C were investigated.

5.4. X-ray diffraction (XRD)

Results of XRD shown in Figs.7(a) Co-26 at.%Ta and (b) Co-27 at.% Ta heat-treated at 1200 °C for 168 h, were identified as diffractions from the λ_3 (C36) and λ_2 (C15) compounds, respectively. Therefore, even though an apparent composition step could not be confirmed at the microstructural boundary in diffusion couples, it can be suggested that a narrow $\lambda_3 + \lambda_2$ two-phase region exists within 26–27 at.% Ta at 1200 °C as marked by a double circle in Fig. 2. The λ_3 (C36) was also identified at 1000 °C and disappeared at 900 °C, which suggests that the eutectoid reaction of λ_3 (C36) = $\chi\text{Co}_7\text{Ta}_2 + \lambda_2$ (C15) occurs between 900 °C and 1000 °C. The eutectoid reaction, $\lambda_1 = \mu + \lambda_2$, is considered to occur at 1130 °C in the phase diagram shown in Fig. 1. As shown in Fig. 7(c and d), however, the λ_1 phase identified in Co-42 at.%Ta heat-treated at 1300 °C transformed into the λ_2 phase at 1290 °C, which suggests that the eutectoid reaction occurs below 1300 °C and above 1290 °C.

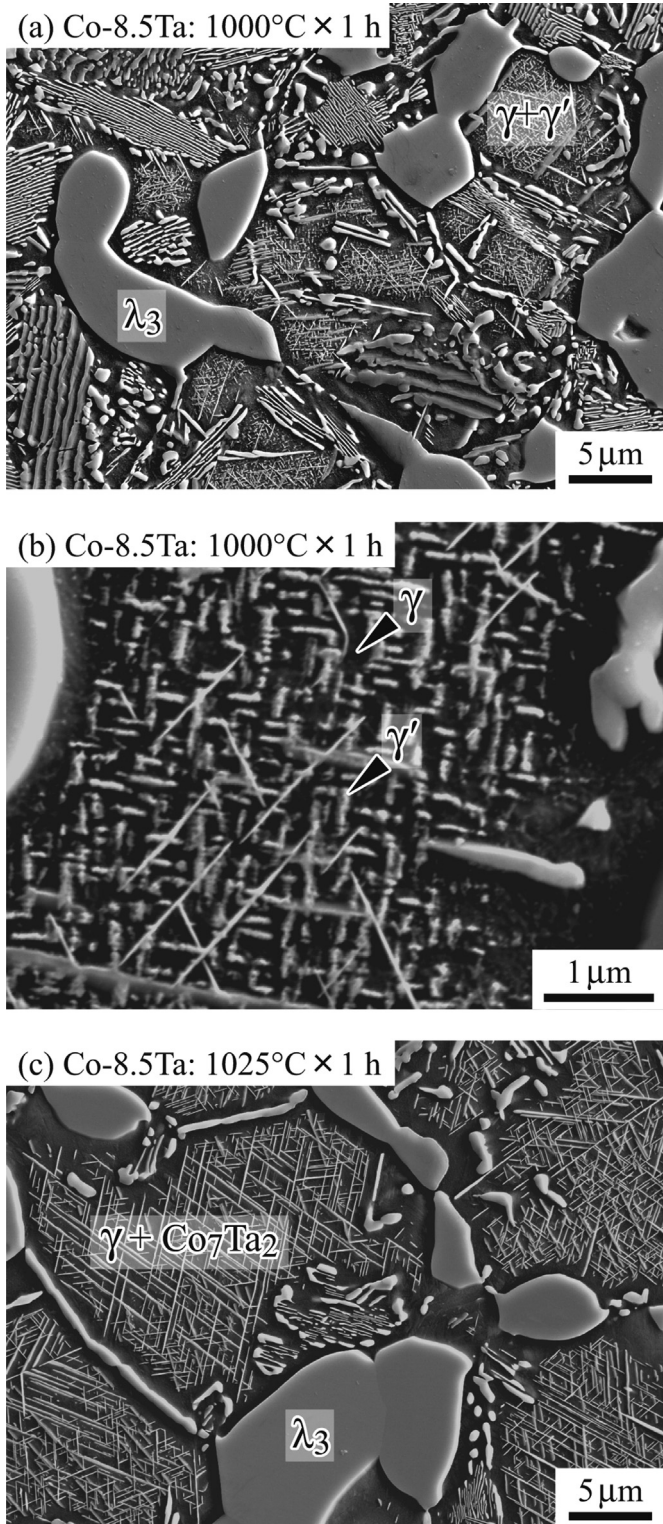


Fig. 9. FE-SEM images of Co-8.5Ta alloy heat-treated at (a), (b) 1000 °C for 1 h and (c) 1025 °C for 1 h.

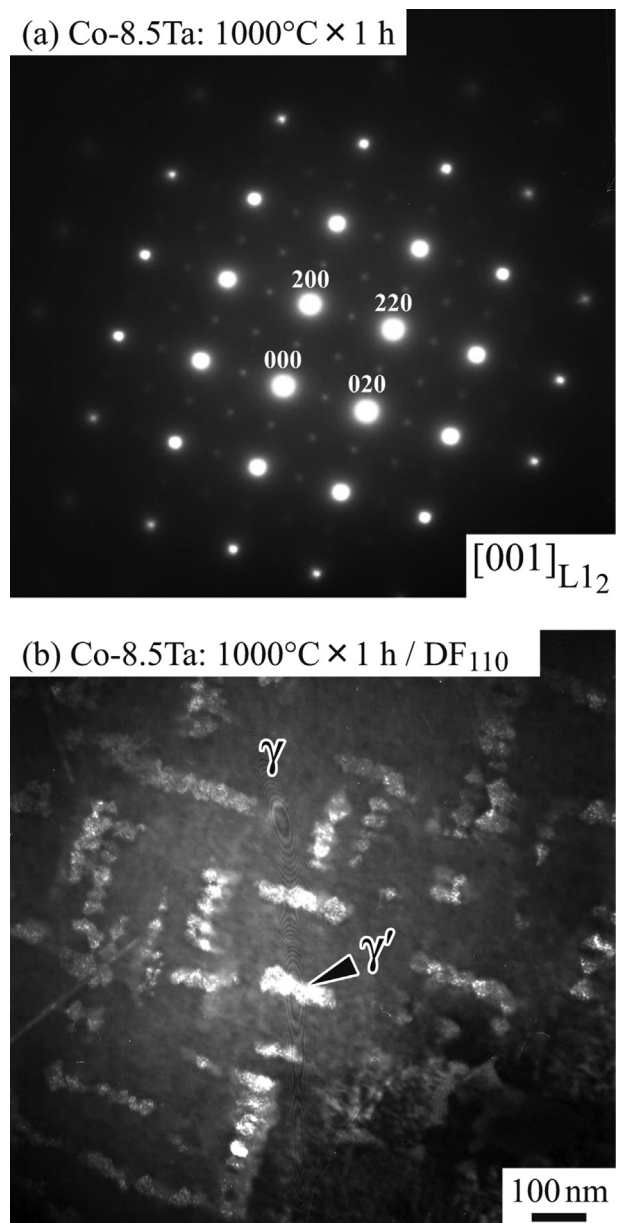


Fig. 10. (a) Electron diffraction pattern and (b) dark field image taken from (110) super reflection of Co-8.5Ta alloy heat-treated at 1000 °C for 1 h.

5.5. Equilibrated microstructures

Fig. 8 shows typical back-scattered electron (BSE) images of equilibrated Co–Ta alloys. The equilibrium composition and crystal structure of each phase were examined by EPMA and XRD, respectively. Results of EPMA measurement are summarized in Table 3 and plotted with open diamonds in Fig. 2. The difference in the equilibrium compositions of the λ_2 phase in Fig. 8(d) and of the λ_1 phase in Fig. 8(e) also confirms the eutectoid reaction and its temperature between those two conditions.

5.6. Metastable γ' phase

According to the result of DSC measured in 8.5 at.% Ta alloy shown in Fig. 4(b), a small signal which may correspond to the dissolution of a certain phase was detected at 1013 °C. To identify the reaction, the microstructure of 8.5 at.% Ta alloys heat-treated at 1000 °C and 1025 °C for 1 h after solution treated at 1300 °C for 120 h was examined by FE-SEM (JEOL JSM-6500F) and TEM (JEOL JEM-2000EXII). The microstructure solution treated at 1300 °C consists of massive particles of λ_3 (23.2 at.%Ta) precipitated in the γ (Co) matrix (5.8 at.%Ta), as shown in Fig. 8(b). In the microstructure quenched from 1000 °C shown in Fig. 9(a), the massive particles of λ_3 remain as they were at 1300 °C. On the other hand, some of the γ (Co) matrix transformed into lamellar domains of γ (Co) + λ_3 by discontinuous precipitation of γ (Co) = γ (Co) + λ_3 . In addition to these two structures, there are domains with complex precipitates, as shown in Fig. 9(b), which consist of needle-like precipitates of χ Co₇Ta₂ and fine chained precipitates dispersed in the γ (Co) matrix of 5.8 at.%Ta. In the same alloy heat-treated at 1025 °C, the fine chained precipitates disappeared as shown in Fig. 9(c), which indicates that the small signal detected at 1013 °C by the DSC shown in Fig. 4(b) was caused by dissolution of these chained precipitates in the 5.8 at.%Ta γ (Co) phase. Fig. 10(a) shows a diffraction pattern taken from these

precipitates together with the γ (Co) matrix phase, in which the super-lattice reflections due to the L1₂ ordered structure (γ' Co₃Ta) in addition to the basic reflections of the disordered fcc phase (γ (Co)) were confirmed. A dark-field image taken from the (110) super-lattice reflection shown in Fig. 10(b) clearly exhibits fine chained particles of the ordered γ' Co₃Ta phase. Results of these TEM examinations suggest that the fine chained precipitates are identified as being the γ' Co₃Ta (L1₂) phase, which seems to be metastable taking into account other experimental results.

5.7. Thermodynamic calculation

Based on the present and previous experimental data, the thermodynamic parameters of stable and metastable phases in the Co–Ta binary system were evaluated using Thermo-Calc software [36]. Optimized parameters are listed in Table 4. The calculated Co–Ta phase diagram compared with experimental data is shown in Fig. 11(a), which indicates that sufficient consistency between calculated and experimental results was obtained. In order to evaluate the stability of the γ' Co₃Ta (L1₂) phase, solvus temperatures of the γ' phase of γ + γ' microstructure (3.5 and 5.8 at.%Ta) shown in Fig. 4(b) as well as the enthalpy of formation of the γ' Co₃Ta (L1₂) phase calculated by *ab-initio* method (–23.44 kJ/mol) [15] were taken into account in this thermodynamic assessment. Fig. 11(b) shows metastable phase equilibria between the γ (Co) (A1) phase and the γ' Co₃Ta (L1₂) phase calculated without taking other phases into account, which suggests that the stoichiometric Co₃Ta phase is stable below 2000 °C. According to the present thermodynamic assessment, the enthalpy of formation was calculated to be –23.87 kJ/mol, which is in good agreement with the *ab-initio* value. This indicates that both the present CALPHAD assessment based on experimental results and the *ab-initio* calculation are trustworthy for investigation of the stability of the metastable γ' Co₃Ta (L1₂) phase.

Table 4

Thermodynamic parameters of the Co–Ta binary system evaluated in this study. Lattice stabilities of pure elements are taken from Ref. [31].

Thermodynamic parameters, G and L [J/mol], and magnetic parameters, T_C [K] and β [μ_B]	
Liquid: (Co, Ta)	
${}^0L_{Co,Ta}^L = -199948.7 + 44.5468 T$, ${}^1L_{Co,Ta}^L = -13651.5$, ${}^2L_{Co,Ta}^L = +38187.4$	
γ (Co) (A1): (Co, Ta) ₁ (Va) ₁	
${}^0L_{Co,Ta}^\gamma = -116349.4$, ${}^1L_{Co,Ta}^\gamma = +18595.2$	
$T_C^\gamma = 1396 \cdot x_{Co}$, ${}^0T_{Co,Ta}^\gamma = -2200$, ${}^1T_{Co,Ta}^\gamma = -804$, $\beta^\gamma = 1.35 \cdot x_{Co}$	
α (Ta) (A2): (Co, Ta) ₁ (Va) ₃	
${}^0L_{Co,Ta}^\alpha = -95196.5 + 18.5567 T$, ${}^1L_{Co,Ta}^\alpha = -3489.72$, ${}^2L_{Co,Ta}^\alpha = +35362$	
$T_C^\alpha = 1450 \cdot x_{Co}$, $\beta^\alpha = 1.35 \cdot x_{Co}$	
ϵ (Co) (A3): (Co, Ta) ₁ (Va) _{0.5}	
${}^0L_{Co,Ta}^\epsilon = -102000 + 15 T$, $T_C^\epsilon = 1396 \cdot x_{Co}$, $\beta^\epsilon = 1.35 \cdot x_{Co}$	
γ' Co ₃ Ta (L1 ₂): (Co, Ta) _{0.75} (Co, Ta) _{0.25} (metastable)	
$\Delta G_{Co_3Ta}^{\gamma'} = -9977.3$	
λ_1 (C14): (Co, Ta) _{0.6667} (Co, Ta) _{0.3333}	
$G_{Co:Co}^{\lambda_1} = +7136.18 + {}^\circ G_{Co}^e$, $G_{Co:Ta}^{\lambda_1} = -47822.4 + 8.25972 T + 0.6667 {}^\circ G_{Co}^e + 0.3333 {}^\circ G_{Ta}^e$	
$G_{Ta:Ta}^{\lambda_1} = +43644.4 + {}^\circ G_{Ta}^e$, $G_{Ta:Co}^{\lambda_1} = +0.3333 {}^\circ G_{Co}^e + 0.6667 {}^\circ G_{Ta}^e$, ${}^0L_{Co:Ta}^{\lambda_1} = -57521.2$	
λ_2 (C15): (Co, Ta) _{0.6667} (Co, Ta) _{0.3333}	
$G_{Co:Co}^{\lambda_2} = +6000 + {}^\circ G_{Co}^e$, $G_{Co:Ta}^{\lambda_2} = -48641.8 + 8.4912 T + 0.6667 {}^\circ G_{Co}^e + 0.3333 {}^\circ G_{Ta}^e$	
$G_{Ta:Ta}^{\lambda_2} = +3000 + {}^\circ G_{Ta}^e$, $G_{Ta:Co}^{\lambda_2} = +0.3333 {}^\circ G_{Co}^e + 0.6667 {}^\circ G_{Ta}^e$, ${}^0L_{Co:Co:Ta}^{\lambda_2} = -4140.21$	
λ_3 (C36): (Co, Ta) _{0.6667} (Co, Ta) _{0.3333}	
$G_{Co:Co}^{\lambda_3} = +6000 + {}^\circ G_{Co}^e$, $G_{Co:Ta}^{\lambda_3} = -48453.85 + 8.445 T + 0.6667 {}^\circ G_{Co}^e + 0.3333 {}^\circ G_{Ta}^e$	
$G_{Ta:Ta}^{\lambda_3} = +3000 + {}^\circ G_{Ta}^e$, $G_{Ta:Co}^{\lambda_3} = +0.3333 {}^\circ G_{Co}^e + 0.6667 {}^\circ G_{Ta}^e$, ${}^0L_{Co:Co:Ta}^{\lambda_3} = -4743.62$	
μ (D8 _b): (Co) _{0.4615} (Ta) _{0.3077} (Co, Ta) _{0.2308}	
$G_{Co:Ta:Co}^\mu = -28201.5 + 0.6923 {}^\circ G_{Co}^e + 0.3077 {}^\circ G_{Ta}^e$, $G_{Co:Ta:Ta}^\mu = -32926.8 + 0.4615 {}^\circ G_{Co}^e + 0.5385 {}^\circ G_{Ta}^e$	
${}^0L_{Co:Ta:Co:Ta}^\mu = -44515.8 + 22.594 T$	
CoTa ₂ (C16): (Co, Ta) _{0.3333} (Co, Ta) _{0.6667}	
$G_{Co:Co}^{CoTa_2} = +5000 + {}^\circ G_{Co}^e$, $G_{Co:Ta}^{CoTa_2} = -25117.1 + 0.3333 {}^\circ G_{Co}^e + 0.6667 {}^\circ G_{Ta}^e$	
$G_{Ta:Ta}^{CoTa_2} = +5000 + {}^\circ G_{Ta}^e$, $G_{Ta:Co}^{CoTa_2} = +0.6667 {}^\circ G_{Co}^e + 0.3333 {}^\circ G_{Ta}^e$	
${}^0L_{Co:Co:Ta}^{CoTa_2} = -44063.2$, ${}^0L_{Co:Ta:Ta}^{CoTa_2} = +9378.2$	
χ Co ₇ Ta ₂ : (Co) _{0.7778} (Ta) _{0.2222} $\Delta G_{Co_7Ta_2}^\chi = -33091.5 + 5.16 T$	

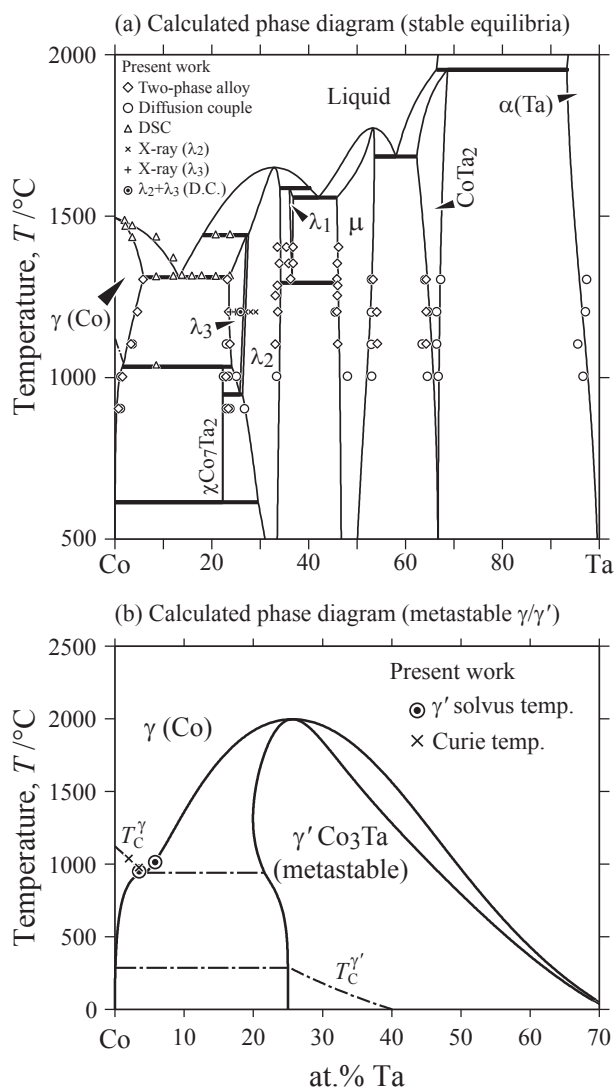


Fig. 11. Calculated phase diagram of the Co–Ta system; (a) stable phase equilibria compared with experimental data and (b) metastable equilibrium between γ (Co) and γ' Co₃Ta phases.

6. Conclusion

Experimental investigation and thermodynamic calculation of the phase diagram of the Co–Ta binary system was carried out. Equilibrium compositions appeared in two-phase alloys and diffusion couples were determined by EPMA at temperatures between 900 °C and 1450 °C. In the diffusion couples, neither composition steps nor changes of the slope in the composition profile which correspond to the λ_2 (C15) + λ_3 (C36) two-phase region could be observed. Across a composition, Co–26.5 at.%Ta, in the profile, however, the microstructure changes drastically, which suggests that the equilibrium phases change in composition from λ_3 (C36) to λ_2 (C15) with increasing Ta content. A very narrow λ_3 (C36) + λ_2 (C15) two-phase region is considered to exist around 26.5 at.% Ta at temperatures between 950 °C and 1448 °C according to these results. Primary crystals and invariant reactions which appeared during solidification were identified by microstructure examinations of as-cast Co-(24–60 at.%)Ta alloys, yielding

information to construct equilibrium relationships among the liquid, Laves (λ_1 (C14), λ_2 (C15), λ_3 (C36)), μ and CoTa₂ phases above 1500 °C. The solvus temperature of the γ' (L1₂) phase in the 5.8 at.% Ta γ (A1) phase and that of the peritectoid reaction of the χ Co₇Ta₂ phase in a Co–8.5 at.%Ta alloy were determined to be 1013 °C and 1033 °C by DSC, respectively. According to the results of TEM observation, it is concluded that the γ' Co₃Ta (L1₂) phase is metastable in this binary system. The calculated phase diagram shows good agreement with the experimental phase diagram revised in the present study. The metastable γ' Co₃Ta (L1₂) stoichiometric compound phase was estimated to be disordered at 2000 °C. The evaluated enthalpy of formation of the metastable γ' Co₃Ta ($\Delta H(\gamma'Co_3Ta) = -23.86$ kJ/mol) is consistent with the *ab initio* calculation (-23.44 kJ/mol), which might provide essential information on the effect of Ta on the Co–Al–W-base superalloys.

Acknowledgments

The authors wish to thank Dr. Nagasaki for his experimental support of the TEM examination. This work was supported by a Grant-in-Aid for Scientific Research from the Japan Society for the Promotion of Science and by a Grant for Excellent Graduate Schools from MEXT, Japan. Support from New Energy and Industrial Technology Development Organization (NEDO) is also acknowledged.

References

- [1] Sims CT, Stoloff NS, Hagel WC. Superalloys II. New York: John Wiley & Sons; 1987.
- [2] Bradley AJ, Seager GC. J Inst Met 1939;64:81–91.
- [3] Edwards OS. J Inst Met 1941;67:67–77.
- [4] Omori T, Sutou Y, Oikawa K, Kainuma R, Ishida K. Mater Sci Eng A 2006;438–440:1045–9.
- [5] Drapier JM, de Brouwer JL, Coutouradis D. Cobalt 1965;25:59–72.
- [6] Drapier JM, Coutouradis D. Cobalt 1968;39:63–74.
- [7] Dutkiewicz J, Kostorz G. Acta Metall Mater 1990;38:2283–6.
- [8] Dutkiewicz J, Kostorz G. Mater Sci Eng A 1991;A132:267–72.
- [9] Sato J, Ohmori T, Oikawa K, Ohnuma I, Kainuma R, Ishida K. Science 2006;312:90–1.
- [10] Miura S, Ohkubo K, Mohri T. Mater Trans 2007;48:2403–8.
- [11] Shinagawa K, Omori T, Sato J, Oikawa K, Ohnuma I, Kainuma R, et al. Mater Trans 2008;49:1474–9.
- [12] Jiang C. Scr Mater 2008;59:1075–8.
- [13] Chen M, Wang CY. Scr Mater 2009;60:659–62.
- [14] Ooshima M, Tanaka K, Okamoto NL, Ishida K, Inui H. J Alloys Compd 2010;508:71–8.
- [15] Omori T, Oikawa K, Sato J, Ohnuma I, Kattner UR, Kainuma R, et al. Intermetallics 2013;32:274–83.
- [16] Suzuki A, Pollock TM. Acta Mater 2008;56:1288–97.
- [17] Okamoto H. J Phase Equilibria Diffus 2004;25:571–2.
- [18] Hashimoto U. Nippon Kinzoku Gakkai-Shi 1937;1:177–90.
- [19] Koster W, Mulfinger W. Z Met 1938;30:348–50.
- [20] Petkov VV, Kocherzhinsky YA, Markiv VY. Fiziko-Tekhnichni Ta Matermetichni Nauki; 1971. pp. 852–4.
- [21] Petkov VV, Kocherzhinsky YA, Markiv VY. MetallofizikaUSSRSSSR; 1972. pp.93–7.
- [22] Bernard VB, Yurchenko LA, Bodak OI, Kuprina VV. Vestn Mosk Univ Khim 1976;17:208–12.
- [23] Korshynsky M, Fountain RW. Trans AIME 1959;213:1033–43.
- [24] Kaufman L. CALPHAD 1991;15:243–59.
- [25] Niessen AK, de Boer FR, Boom R, de Chatel PF, Mattens WCM, Miedema AR. CALPHAD 1983;7:51–70.
- [26] Colinet C, Pasturel A, Hicter P. CALPHAD 1985;9:71–99.
- [27] Liu ZK, Chang YA. CALPHAD 1999;23:339–56.
- [28] Hari-Kumar KC, Van Rompaey T, Wollants P. Z Met 2002;93:1146–53.
- [29] Hari-Kumar KC, Ansara I, Wollants P. CALPHAD 1998;22:323–34.
- [30] Joubert JM, Dupin N. Intermetallics 2004;12:1373–80.
- [31] Dinsdale AT. Calphad 1991;15:317–425.
- [32] Inden G. Report of the project meeting CALPHAD V. Dusseldorf; 1976. III.4–1.
- [33] Inden G. Physica 1981;103B:82–100.
- [34] Hillert M, Jarl M. CALPHAD 1978;2:227–38.
- [35] Ansara I, Dupin N, Sundman B. CALPHAD 1997;21:535–42.
- [36] Sundman B, Jansson B, Andersson JO. CALPHAD 1985;9:153–90.